

Dynamic Control Allocation between Onboard and Delayed Remote Control for Unmanned Aircraft System Detect-and-Avoid

Asma Tabassum^{a,*}, He Bai^a

^a*Department of Mechanical and Aerospace Engineering, Oklahoma State University*

Abstract

This paper develops and evaluates the performance of an allocation agent to be potentially integrated into the onboard Detect and Avoid (DAA) computer of an Unmanned Aircraft System (UAS). We consider a UAS that can be fully controlled by the onboard DAA system and by a remote human pilot. With a communication channel prone to latency, we consider a mixed initiative interaction environment, where the control authority of the UAS is dynamically allocated by the allocation agent. In an encounter with a dynamic intruder, the probability of collision may increase in the absence of pilot commands in the presence of latency. Moreover, a delayed pilot command may not result in safe resolution of the current scenario and need to be improvised. We design an optimization algorithm to reduce collision risk and refine delayed pilot commands. Towards this end, a Markov Decision Process (MDP) and its solution are employed to create a wait time map. The map consists of estimated times that the UAS can wait for the remote pilot commands at each state. A command blending algorithm is designed to select an avoidance maneuver that prioritizes the pilot intention extracted from the pilot commands. The wait time map and the command blending algorithm are implemented and integrated into a closed-loop simulator. We conduct ten thousands fast-time Monte Carlo simulations and compare the performance of the integrated setup with a standalone DAA setup. The simulation results show that the allocation agent enables the UAS to wait without inducing any near mid air collision (NMAC) and severe loss of well clear (LoWC) while positively improve pilot involvement in the encounter resolution.

Keywords: Unmanned aircraft system; Dynamic control allocation; Detect and Avoid

1. Introduction

In this era of cutting edge Artificial Intelligence, implementation of intelligent software agents and advent of advanced algorithms are making autonomous vehicles more adaptive to uncertainties and anomalies. Human computer interaction studies aim to leverage a human's ability to aid in the execution of autonomous actions while ensuring the best experience for a human operator. The balance between the two different paradigms, namely autonomous control and human control, falls into the mixed-initiative interaction paradigm [1]. Marti et

*Graduate Research Assistant
E-mail address: asma.tabassum@okstate.edu

al. [1] describe mixed-initiative interaction as a *"Flexible interaction strategy in which each agent (human or autonomous system) contributes what it is best suited at the most appropriate time"*. This allows an autonomous system working with a human to develop a shared understanding of the goals and of contributing to the problem solving in the most appropriate way. In a generic situation, the disengage and reengage of the autonomous system can be initiated manually. However, for a safety critical system in the presence of anomaly, uncertainty and obstacles, manual transition of the command may lead to undesired consequences. Often times an operator requires some advisory and needs a considerable amount of time to take over control as the situation demands [2], which may lead to non-smooth or bumpy transitions [3]. This establishes the necessity of designing efficient algorithms to allocate and blend the commands based on the quantitative as well as the qualitative analysis of the proposed actions. When designing such a controller scheme, the ultimate goal, constraints and cost functions vary in a wide range depending on the applications.

For aerospace applications, optimization and control design for a standalone airborne system itself demands more scrutiny and requires guaranteed operability in a dynamic environment. This becomes more challenging for a UAS, where a remote pilot does not have the provision of analyzing the dynamic environment onboard. Therefore, the task to develop a control scheme that can dynamically allocate control authority between the pilot and the DAA system as well as adjust both commands to guarantee safe maneuvers and adaptation to uncertainties is challenging.

In this paper, we consider a Detect-and-Avoid problem, where an ownship UAS is in an active encounter with a dynamic intruder. The UAS is remotely controlled by a pilot at the Ground Control Station (GCS). In the presence of the communication latency, the UAS needs to make decisions on 1) whether it can wait for pilot commands given the current encounter and 2) how to integrate the delayed pilot commands when received. To answer these questions, we employ a dynamic control allocation agent to ensure effective authority transition in the encounter. Without redesigning the onboard DAA system, we implement a decision-theoretic approach to effectively increase the remote pilot's contribution within safe operational conditions and enhance human-machine user experience. In particular, we employ a Markov Decision Process (MDP) to generate a dynamic waiting strategy for the ownship UAS when pilot commands are unavailable due to latency. One of the benefits of waiting is that if the pilot's maneuver commands are received while the UAS is waiting, the intent of the maneuver, e.g., the maneuver types, can be assimilated into the onboard DAA system to generate a maneuver similar to the pilot commands.

We evaluate the competency of the MDP wait map using 10,000 fast-time Monte Carlo simulations. An extensive data analysis is carried out on the simulation data to quantify

the performance and measure the risk associated with the allocation agent. Our results demonstrate noteworthy improvement in the pilot command reception without inducing any near-mid-air collision instances and enhancement of pilot involvement in decision making in the encounter resolution. Utilization of the pilot command has increased by 15.81% with the integrated control allocation agent. On average, the implemented command blending algorithm enables execution of commands in the pilot preferred approach in 84% of the instances. This paper generalizes the 2D MDP approach in [4] to 3D and extends [5] by providing a large scale simulation study and analysis to validate the proposed approach.

The rest of the paper is structured as follows. The rest of the Section 1 discusses the literature and the contribution of this paper. Section 2 presents the problem definition, mathematical formulation of the MDP, and the command blending algorithm. Section 3 provides the simulation parameters, encounter designs and analysis metrics. The simulation results are presented and analyzed in Section 4. Conclusions are provided in Section 5.

1.1. Literature Review

In a shared control architecture, both the autonomous system and human operator have full authority to steer a dynamical system. In the recent years, several shared control architectures have been proposed based on various coordination and interaction methods, including control authority switch, supervise-assist and command blend. To have an efficient coordination between human and autonomy, studies have been carried out on the transition of the control authority. These studies presented different approaches such as emergency stop, adaptive control, Support Vector Machines (SVM), and Model Predictive Control (MPC) to address different scenarios in diverse operating conditions. Control authority allocation between an autonomous system and a remote human operator demands dynamic optimization with guaranteed operability and safety under a wide range of operating conditions, constraints and uncertainty. Several studies [6, 7, 8, 9, 10] address this problem depending on the system specifications by utilizing existing methods with adaptations for ground and airborne vehicle. The authors [6] develop a simultaneous steering control algorithm using adaptive MPC such that the controller shares control with the driver in a minimally invasive manner while avoiding obstacles and preventing loss of control. The authors [7] employ control switching between a driver and an autonomous system that is triggered by the driver drowsiness analysis. In [8], the authors propose to use an emergency stop as a fallback solution to maintain the vehicle’s safety in case the human operator never responds to a proposition from automation. The authors in [9] propose a switching control method for an autonomous flight controller where a human pilot takes over based on the pilot’s perception of the Capacity of Maneuver of the actuator. Later, they propose transitioning

authority from the autopilot to a more advanced autopilot following the pilot’s perception of an anomaly [10].

Researchers have also considered human as supervisor and autonomous system as assistant, e.g., [11, 12, 13, 14, 15, 16, 17, 18], In [11], a theoretic controller is formulated for shared control of a quadruped rescue robot that composes human inputs with autonomous controls to guide human controlled leg positions. In a subsequent work [12], the authors adopt a “prediction-human” feedback loop by applying a dual-mode MPC technique and search-and-rescue inspired human operator trial. In [13], online evaluation of the human operator’s risk-based performance is employed for bilateral tele-operation of mobile robots to make compensation for their commands in the event of poor operator performance. To keep the safety of the vehicles, the authors [14] propose to model the driver from empirical observations and incorporate the model into a control framework to correct the driver’s input. In [15], the authors propose a model based on supervisor authority over autonomous flight controller during anomaly and validate the model with human-in-the loop simulations. The authors in [16] adopt a shared supervisory architecture in which the adaptive autopilot changes the controller structure and responds accordingly in the event pilot detects any anomaly in flight. In [17], a control framework and its associated experimental test bed for the bilateral shared control of a group of QR UAVs are investigated where a topological motion controller increase the tele-presence of human assistants.

A promising shared control architecture is the command blend architecture [19, 20, 21, 22, 23, 24] where the commands of the human operator and the autonomous system are fused to control the system. A wheelchair shared controller is presented in [19] where the navigation path was adapted with user intention. Reference [20] presents a brain-computer interface for shared control of an wheel chair to perform goal directed navigation and assist human adaptively. The authors in [21] propose to use a Gaussian Mixture Model to learn weighing coefficients to blend the control. Input mixing control is adopted by some studies [22, 23] where human-autonomous commands are blended to determine the final command. The authors in [22] present a methodology of sliding scale autonomy to allow a user to adjust the autonomy of the flying robot. However the human has to know the sliding scale as the environment changes. In [23], the authors calculate a scale factor by minimizing a cost function that incorporates human command, obstacle potential field and obstacle avoidance controller. The scalar blending factor for human-autonomous command blending, α , is used to denote the degree of the authority. The value of α can be set 0 or 1 or changed adaptively [24]. The percentage of α indicates how much control authority should be allocate to human-machine over different operating scenarios. Apart from shared control concept, fault tolerant adaptive controller [25] has been studied with a pilot in the loop simulation to

reduce pilot workload during faulty situations. The authors in [26] consider Pilot Induced Oscillations (PIOs) from the point of view of nonlinear dynamics and nonlinear control in aircraft.

As UAS applications continue to expand, researches have been carried out on the path prediction, tracking and control as well as collision avoidance algorithm development [27, 28, 29, 30, 31, 32, 33, 34]. Detect-and-Avoid concept of operation is illustrated in [35] and several studies [36, 37, 38, 29, 39] specifically focus on the safety critical analysis of a standalone DAA with different methodologies as well as design of cognitive pilot-machine interface [40, 41]. When implementing a shared architecture with UAS DAA, it is important to consider any inconsistency or latency that exists in the communication channel, since communication is crucial for sending surveillance information to ground control station and receiving pilot command. According to [42], latency can be described as one of the most significant factors for instability and performance degradation. In [43], the authors show a simulated communication loss at air traffic network increases conflict rates beyond the baseline level within 1 minute of the failure and that increased by at least a factor of 4 within 5 minutes of the communication failure. For flight control system, latency or delay influences flying quality and reliability of the operation and requires substantial effort to restore [44]. Also in [45], the authors demonstrate how long range network latency causes reduced control performance as well as instability of the UAS. The authors design classical PID to compensate for the effects of time delay and stabilize the vehicle. A sensitivity analysis has been carried out in [46] that analyzes the intolerances of possible delays in control-input command with respect to the navigation performance on a fixed-wing unmanned aerial system and states that a rapid growth of position error even for delays as small as ten of milliseconds may directly affect the situational awareness. To compensate for the latency in bilateral tele-operation of a UAS, the authors in [47] propose to use proportional plus damping injection (P+D) controller to increase the system stability. In [48], the authors consider obstacle avoidance for tele-operated UAVs with time delays and evaluates the effectiveness of using wave variables in haptic feedback to improve operators' avoidance performance. The authors in [49] demonstrate how to use analytical solutions for ODEs and DDEs to estimate the time delay in Internet-based feedback control and quadrotor types of UAS. A feedback augmentation method is illustrated in [50] where the estimate of the change in the vehicle state due to the commands that are yet to affect the feedback is computed. This feedback received by the pilot is modified to reflect the predicted change. This way the pilot becomes aware of the effect of the control inputs immediately.

1.2. Contribution

Although the existing control allocation and shared control architectures have considered diverse ranges of operating conditions, including vehicle dynamics, anomalies and sensor uncertainties, communication latency has not been considered extensively, which is the main focus of this paper. The existing literature for airborne platforms consider the supervisor-assist [51, 16, 52] control architecture in the presence of anomalies where we consider a allocation-blend architecture that connects degraded pilot’s situational awareness unlike the standalone baseline setup. The proposed architecture is capable of both control transition and command blend in a dynamic environment with communication latency. The control allocation agent dynamically allocates the control authority between the onboard DAA and the pilot and is separate from the autonomous system and the human operator. Although a control allocation agent has been successfully implemented in many complex distributed control plants including but not limited to electro-hydraulic driven devices and industrial robots [53, 54, 55, 56], airborne vehicles [57, 58, 59] and in multi-agent network [60] implementation in an unmanned aircraft mixed initiative application is very limited. This paper defines a mixed initiative infrastructure that utilizes MDP wait maps, current relative states, pilot commands and DAA commands to safely authorize pilot or DAA to take over the control as well as incorporate the pilot intention. The developed wait map is designed to ensure safe navigation when the allocation agent holds the authority and blend pilot intended maneuver into the resolution. The efficiency of the MDP wait map and competence of the allocation agent are investigated through 10,000 fast-time Monte Carlo simulations that encompass a wide range of encounter geometry. The results show positive improvement in pilot command involvement and produce an average increase of 15.81% of the utilization of pilot commands than a standalone DAA architecture. Furthermore, none of the simulations has induced NMAC instances.

2. Problem Formulation

Consider an ownship UAS whose communication channel to and from the GCS suffers from latency during an encounter with a dynamic intruder aircraft. The round-trip latency duration can be in the range of 0.2 to 10 seconds [35]. As the onboard surveillance system detects the intruder, the surveillance information is transmitted to the pilot at the GCS. The remote pilot from the GCS takes a maneuver decision and sends commands back to the UAS. We assume that the onboard DAA system is also capable of generating and executing avoidance maneuvers. However, these maneuvers may be significantly different from the maneuvers generated by the pilot. On the other hand, the pilot command may not be received by the UAS prior to a resolution maneuver time frame. To improve pilot-UAS

interaction experience, it may be desirable to hold control authority for pilot over computer. However, in the event of latency, waiting for remote pilot's commands may significantly increase the risk of collision.

We propose a control allocation agent that utilizes a prior waiting map solved from a MDP model. The MDP is developed in 3-D dimension and based on the ownship and intruder initial state and the intruder dynamic motion model. The solution to the MDP acts as prior information for the agent to decide how long the UAS can wait for the pilot's commands before the onboard DAA is authorized to take over. We next discuss how the MDP is formulated and the design of the control allocation agent.

2.1. Formulation of the MDP

A generic MDP can be defined as a tuple (S, A, P, R) [61], where S is the state space, A is the action space, P is the transition probability and R is the reward function. We describe the relationship between the UAS and an intruder in a relative coordinate system. A kinematic model for both the UAS and the intruder is adopted from [62]. In our study, the state space has six states: relative distance in the x dimension, ΔX , relative distance in the y dimension, ΔY , relative altitude, d_h , intruder horizontal speed, v_i , relative vertical velocity, V_h , and intruder heading, θ_i . The states are updated as

$$\Delta X(t + \Delta T) = \Delta X(t) + V_{rx}(t)\Delta T \quad (1)$$

$$\Delta Y(t + \Delta T) = \Delta Y(t) + V_{ry}(t)\Delta T \quad (2)$$

$$d_h(t + \Delta T) = d_h(t) + V_h(t)\Delta T \quad (3)$$

$$v_i(t + \Delta T) = v_i(t) + \Delta v_i(t)\Delta T \quad (4)$$

$$\theta_i(t + \Delta T) = \theta_i(t) + \Delta\theta_i(t)\Delta T \quad (5)$$

$$V_h(t + \Delta T) = V_h(t) + \Delta v_h(t)\Delta T, \quad (6)$$

where ΔT is the transition time and we set $\Delta T = 1$ second. The values of V_{rx} and V_{ry} are calculated as

$$V_{rx}(t) = v_i(t) \cos \theta_i(t) - v_o(t) \cos \theta_o(t) \quad (7)$$

$$V_{ry}(t) = v_i(t) \sin \theta_i(t) - v_o(t) \sin \theta_o(t) \quad (8)$$

where v_o and θ_o are the ownship horizontal speed and heading, respectively.

State transition probability depends on the action taken by the UAS and the probability of the intruder dynamics. We use a preset intruder motion model to compute the transition of the MDP. Table 1 illustrates the intruder motion model, m_i . Equation 1–6 can be described by a generic discretized state space model as:

$$S(k + 1) = f(S(k), u_a(k), \Delta v_i, \Delta\theta_i, \Delta v_h) \quad (9)$$

Table 1: Intruder Motion Model, m_i

Vertical dynamics	Probability	Horizontal dynamics	Probability	Turn rate dynamics	Probability
Δv_h (m/s ²)	$P(\Delta v_h)$	Δv_i (m/s ²)	$P(\Delta v_i)$	$\Delta \theta_i$ (deg/s)	$P(\Delta \theta_i)$
-5	0.15	-10	0.10	-5	0.20
-3	0.20	-5	0.15	-2.5	0.20
0	0.30	-2.5	0.15	0	0.20
3	0.20	0	0.20	2.5	0.20
5	0.15	2.5	0.15	5	0.20
		5	0.15		
		10	0.10		

where $S(k) \in R^{6 \times 1}$ is the current state, $u_a(k)$ is the current input command that includes the current ownship airspeed, heading and vertical velocity, which are assumed available, and $\Delta v_i, \Delta \theta_i, \Delta v_z$ are drawn from the intruder motion model m_i in Table 1. Equation 9 describes the discrete state transition depending on the current state $S(k)$ given $u_a(k)$ and the intruder maneuvers randomly drawn from Table 1.

We include two more special states named *Out* state and the *LoWC* state. The *Out* state is the state after the UAS takes an evasive maneuver and after this the MDP will be terminated. The *LoWC* state is the state where the UAS and the intruder have a distance smaller than a preset threshold. It is an event in which a UAS is in close proximity with another aircraft such that the following three conditions are concurrently true [35]:

$$d_h \leq d_h^* \quad (10)$$

$$HMD \leq HMD^* \quad (11)$$

$$0 \leq \tau_{mod} \leq \tau_{mod}^* \quad (12)$$

where the asterisked parameters are thresholds later described as $LoWC_{threshold}$ and non-asterisked parameters are measured values, d_h is the vertical separation, HMD is the horizontal miss distance and τ_{mod} is the modified *tau*. HMD is the projected separation in the horizontal dimension at the predicted closest point of approach. The mathematical definition is provided in [35].

The action space A consists of two decisions: evasive maneuver and wait. We define $A = \{0, 1\}$, where $A = 0$ refers to wait and $A = 1$ refers to taking an evasive maneuver from the onboard DAA system. The MDP compares state transitions towards the Out state with other discrete states in terms of reward and decides if an evasive maneuver should be taken. For simplicity, we assume that the intruder will take only the vertical or the horizontal maneuver at one time. For the horizontal maneuvers, we consider each possible pair of horizontal speed and turn rate that may be taken by the intruder and compute their probabilities as the product of their probabilities in the intruder dynamic model, m_i in Table

1. Let p_i be the probability of the intruder motion expressed as

$$p_i(m_i) = \begin{cases} P(\Delta v_i)P(\Delta\theta_i) & \text{during horizontal maneuver,} \\ P(\Delta v_z) & \text{during vertical maneuver.} \end{cases} \quad (13)$$

The transition probability for the actions are computed by:

$$P(S'|S, A) = \begin{cases} \sum_{m_i} P(S'|S, A, m_i)p_i(m_i) & \text{if } A = 0 \\ P(S' = out|S, A, m_i) = 1 & \text{if } A = 1 \end{cases} \quad (14)$$

where m_i is the intruder motion model in Table 1.

Each state transition is associated with a reward value depending on the action. The reward function for the wait action is based on the loss of well clear and given by

$$R_w(S', S, A = 0) = -\min\left(\frac{C_1}{HMD(S')}, \frac{C_2}{d_h(S')}\right) + C_3\Delta T \quad (15)$$

where C_1 , C_2 , and C_3 are positive user defined parameters. In this study, we use $C_1 = HMD^* = 1220$, $C_2 = d_h^* = 122$ and $C_3 = 1$. The first term in (15) penalizes close encounters and while the second term encourages waiting. The values of C_1 , C_2 and C_3 are chosen such that whenever the encounter gets too close or potentially violates well clear, the reward will be negative for the waiting action. At all times, taking evasive action will receive zero reward, i.e.,

$$R_e(S', S, A = 1) = 0. \quad (16)$$

Thus, at each time, the reward is given by

$$R(S', S, A) = \begin{cases} R_w & \text{if } A = 0 \\ R_e & \text{if } A = 1. \end{cases} \quad (17)$$

The ownship UAS will receive a positive reward until the distance falls below a certain threshold. In the event when the intruder is in the close proximity, the reward for $A = 0$ will be negative whereas the reward for $A = 1$ will be zero. Therefore, the UAS prefers an evasive action.

To solve for the optimal action at each state, a value function is computed using dynamic programming based on value iteration. The value function is given by

$$V^*(S(k)) = \max_{a(k) \in A} \left(R(a(k)) + \gamma \sum_{S(k+1) \in S} P(S(k+1)|S(k), a(k))V^*(S(k+1)) \right) \quad (18)$$

$\forall S(k) \in S$, where $\gamma < 1$ is the discounted factor and R is the reward function. Using the value iteration algorithm, a discounted MDP is solved and the optimal action (wait or maneuver) is obtained at each state by maximizing the accumulated reward.

The wait time at each state is calculated using weighted transition probabilities. For every state, we propagate every possible path to the *LoWC* state and obtain the corresponding LoWC probability. Assuming that the path is acyclic, the expected waiting time for that state is calculated as the average of the waiting times of all the paths leading to LoWC weighted by their probabilities. A wait map is created by computing the wait time at each state in the map.

2.2. Design of the Control Allocation Agent

We employ an allocation agent which functions separately from the human or the DAA and works as a high level decision maker. The input/output information of the allocation agent is presented in Figure 1. The waiting time map developed from the MDP solutions acts as prior information for the agent. The command allocation at any time depends on the status of pilot command reception, projected loss of well clear $ProjL(\cdot)$ within a look ahead time of N seconds, a safety metric of command $SM(\cdot)$, estimated maneuver time and optimal wait time at the current state. The projected loss of well clear is a function that predicts a loss of well clear within the next N seconds and expressed as

$$ProjL(i) = \begin{cases} 1 & \text{if } \{HMD(i), d_h(i), \tau_{mod}(i)\} \leq LoWC_{threshold} \\ 0 & \text{if } \{HMD(i), d_h(i), \tau_{mod}(i)\} > LoWC_{threshold}; \quad i = 1, \dots, N. \end{cases} \quad (19)$$

When a pilot command is not available, the agent either decides to wait for the pilot command and maintain course, i.e., trajectory from previous pilot commands, or allocate the authority to the onboard DAA for conflict resolution. The wait and no wait decisions are made as

$$W(k) = \begin{cases} Wait & \text{if } w(S(k)) \geq W_T \text{ and } ProjL(i) = 0, \forall i = 1, \dots, N \\ No\ Wait & \text{if } w(S(k)) < W_T \text{ or } ProjL(i) = 1, \exists i \in \{1, \dots, N\} \end{cases} \quad (20)$$

where $w(S(k))$ is the optimal wait time at state $S(k)$ retrieved from the wait map, and W_T is a predetermined wait time threshold. Such a threshold can be chosen based on an estimate of communication latency from available historical data or from a model. Latency of a specific channel can be mathematically modelled [63, 64, 65] or predicted using statistical analysis. Also, the threshold can be determined from available data of the specific aircraft transmitter-receiver. In our simulations, we have chosen $W_T = 4$ sec given delays between 0.2 and 10 seconds.

Prioritizing safety, Equation 20 presents two logical decisions on waiting or not. If at any time, the wait time at the current state is greater than or equal to time threshold and no loss of well clear is projected within the next N seconds, the agent holds the authority for pilot. Although the wait time map was created with *LoWC* penalty, we have added the *LoWC* projection logic to create safeguard. On the other hand, if at any time, the wait time is less

than the threshold time which implies a delayed pilot command may not be available within a specific wait time, or there is a projected *LoWC* within N seconds, the agent authorizes the onboard DAA to take over the control.

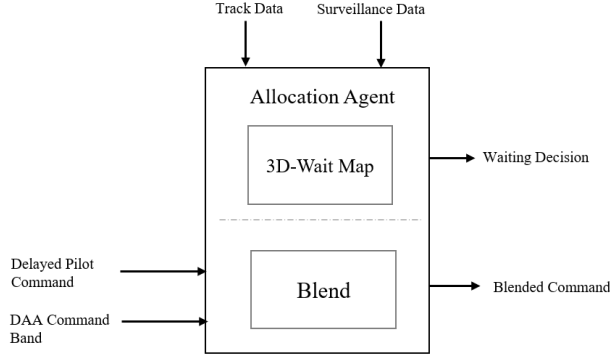


Figure 1: Input/Output diagram for the allocation agent.

When the UAS receives delayed pilot command, the agent optimizes which command to execute to maintain safety as well as enhanced piloting experience. If the UAS receives a delayed pilot command and determines that it is safe to execute that command, the delayed pilot command is implemented. In the case that the received pilot command is not safe evaluated by the safety metric SM , we adopt a blending approach where the preferred maneuver by the pilot is assimilated into DAA maneuver selection. Thanks to the waiting action, the pilot preference can be extracted from the received (delayed) command. Let the received pilot command and the DAA command be u_p and u_{DAA} , respectively. The command allocation algorithm is presented in Algorithm 1.

We now discuss how delayed pilot maneuver commands are employed when they are deemed unsafe. Preference of the pilot maneuver is stored as paired information (ax, d) , where ax refers to the axis or plane of the maneuver, i.e., horizontal or vertical maneuver, and d refers to the direction of the maneuver, i.e., left or right in case of horizontal maneuvers and up and down in case of vertical maneuvers. The agent first searches for a safe avoidance maneuver that matches the pilot preference in terms of maneuver axis and direction. The found maneuver may be more aggressive than the received pilot command due to the latency. If no such safe maneuver is found in the intended direction, the UAS then searches for a safe avoidance maneuver that matches the intended axis. When no safe maneuver can be found to match the intention, the UAS will take any safe maneuver produced by the onboard DAA system. The blending algorithm is described in Algorithm 2.

Algorithm 1 Command allocation algorithm

Input: command reception flag, pilot command u_p , DAA commands u_{DAA} , current intruder state information, current ownship state information.

Output: Avoidance maneuver for the ownship, u_a

if pilot command not received

if $W(k) == Wait$

$u_a \leftarrow u_p$

else if $W(k) == No\ Wait$

$u_a \leftarrow u_{DAA}$

else pilot command received

if $SM(u_p) > 0$

$u_a \leftarrow u_p$

else if $SM(u_p) < 0$

 invoke **Algorithm 2**

Algorithm 2 Command blending algorithm

Input: Extracted (ax, d) , current ownship and intruder state information

Output: Avoidance maneuver for the ownship, u_a

1. Based on the current ownship and intruder state information, search for a safe avoidance maneuver from the onboard DAA system that matches (ax, d)
 2. **if** success **then** *return* the found maneuver as u_a ,
 3. Based on the current ownship and intruder state information, search for a safe avoidance maneuver from the onboard DAA system that matches ax only
 4. **if** success **then** *return* the found maneuver as u_a ,
 5. Based on the current ownship and intruder state information, *return* any safe avoidance maneuver as u_a .
-

3. Simulation Parameters and Analysis Metric

In the development of wait maps, all distances are considered in the relative coordinate system. The UAS position is $(0, 0, 0)$ m and has a constant airspeed of 55 m/s with a heading of 0 degree. The state space ranges from -1500 m to 1500 m for ΔX and ΔY , -200 m to 200 m for d_h , 70 m/s to 300 m/s for v_i and -5 m/s to 5 m/s for V_h . The numbers of bins for discretizing the states are 12, 12, 4, 5, 5, 5, respectively. For any transition, whenever the HMD is less than the HMD threshold and the current vertical separation is less than the vertical separation threshold, the reward will be negative for the waiting action and an evasive action will be taken. We use a publicly available toolbox [66] to solve the MDP. After solving the MDP, we have the optimal decision at each state and then calculate the corresponding wait time.

3.1. Generate the Wait Maps

By changing the intruder initial conditions, we obtain different wait maps. Figure 2 presents a histogram of wait time. The histogram mirrors a left skewed Gaussian distribution. The maximum wait time is 40 seconds and the minimum wait time is 1 second. In most of the states the wait time time ranges between 5 and 10 seconds. A 3-D representation of a wait map is provided in Figure 3.

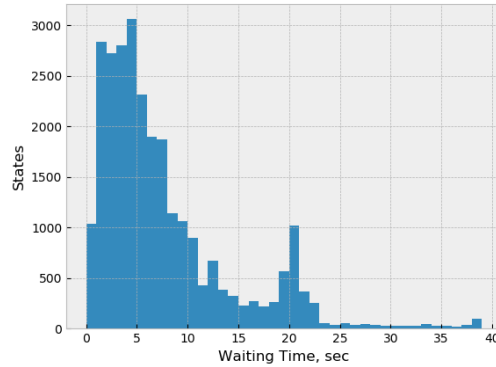


Figure 2: Histogram: Waiting time through out states

The positive relative X range depicts the intruder approaching the UAS, i.e., head-to-head encounters, and the negative relative X range depicts overtaking encounters, i.e., the intruder is approaching the UAS from behind. The wait time is lower in head-to-head encounters than in overtaking encounters. This is because the dynamic collision volume is approaching the intruder and the closure rate is higher. The decrease in the wait time is observed as the relative X distance reduces.

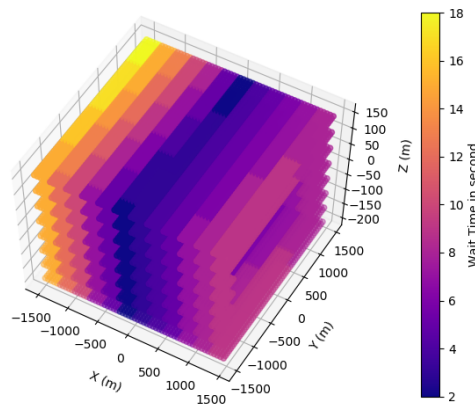


Figure 3: An example of 3D waiting map

Figure 4 represents a top view of the wait map with a non-zero turn rate and illustrates how turn rate impacts the wait time. Comparing the two plots in Figure 4, we see how

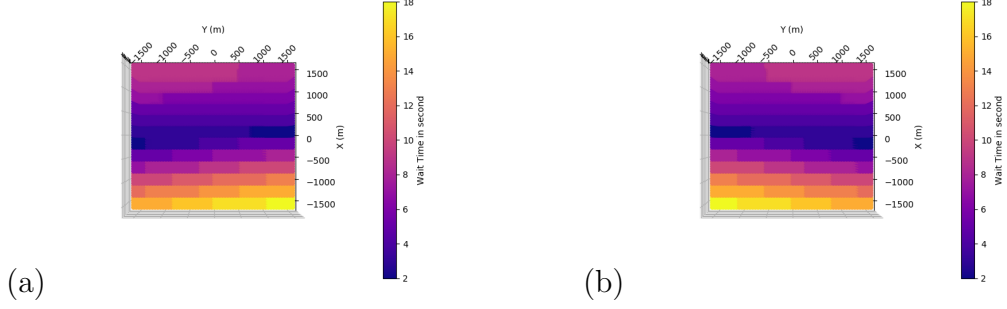


Figure 4: Top View of a wait map, (a) $v_i = 155$ m/s , $\Delta\theta_i = -5$ deg/s, (b) $v_i = 155$ m/s, $\Delta\theta_i = +5$ deg/s. The wait map mirrors as the sign of the turn rate changes to the opposite.

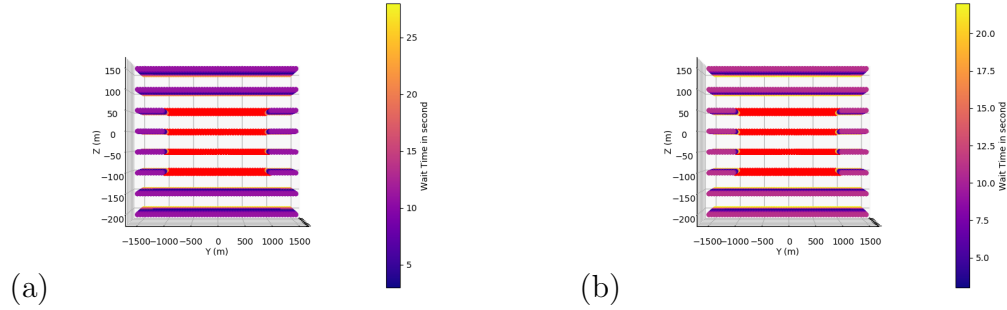


Figure 5: Front view of the wait maps for (a) $v_h = 3$ m/s and (b) $v_h = 5$ m/s within $\Delta X = [-400, -1500]$. The ΔX range has been chosen to illustrate the LoWC region (red area). An increase in the vertical velocity changes the waiting time.

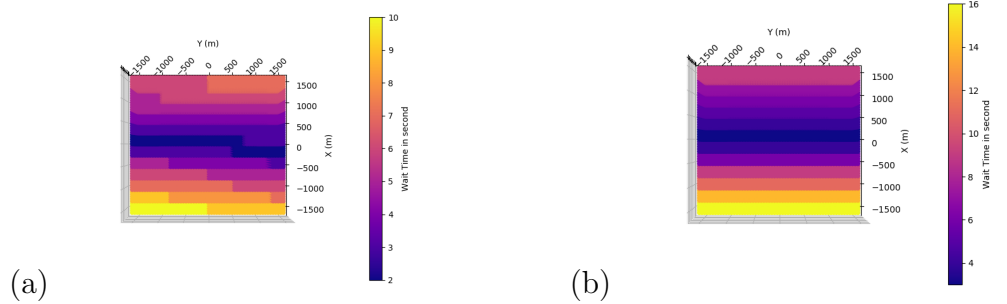


Figure 6: Top View of a wait map (a) $v_i = 300$ m/s , $\Delta\theta_i = 5$ deg/s , (b) $v_i = 155$ m/s , $\Delta\theta_i = 0$ deg/s

alternating turn angle changes the wait time, and the maps are mirror to each other. The positive initial turn leads to less wait time for intruders appearing from the right in head-to-head encounters and from the left in overtaking encounters. On the other hand, a negative turn rate results in less wait time when the intruder converges from the left in head-to-head encounters and from the right in overtaking encounters. The effect of change in vertical speed is presented in two different plots in Figure 5 . The wait time also changes as the relative horizontal speed changes. This can be seen from the two plots in Figure 6, where the first plot has a similar condition to the second plot in Figure 4 except the change in the

horizontal speed. The wait map in Figure 4-b has a higher wait time than the map in Figure 6-a, since the horizontal speed in the latter plot is higher. Figure 6-b represents a zero turn rate which results in a symmetric map. In the case of a non-turning intruder, the wait time also increases with the horizontal speed.

3.2. Encounter Scenarios

The encounter scenarios are representative scenarios from [35]. We have generated 10,000 pairs of aircraft trajectories that encompass a wide range of encounter geometry. For the generation of the trajectories, we consider the ownship flying straight north with a constant velocity. We define the incident angle ia as the angle between the longitudinal axis of the ownship and the intruder in the counter-clockwise direction and the horizontal miss angle hma as the angle between the longitudinal axis of the ownship and the position the intruder. To create turning geometries, we define another parameter ‘advance rate’ that indicates the time to start turn. For example, an advance rate of 0.55 indicates that a turning maneuver of the intruder happens at time $t = 0.55T$ sec, where T is the total encounter time. We set $T = 240$ sec. The intruder parameters used to generate the waypoints are given in Table 2.

Table 2: Intruder Parameters for Trajectory Generation

Parameters	Min	Max	Distribution
Speed (m/s)	70	400	Gaussian(100,30)
vertical velocity (m/s)	-10	10	Gaussian(0,10)
ia (deg)	0	180	30% 180, rest uniform
hma (deg)	-110	110	Gaussian(0,110)
HMD (m)	0	2750	uniform
VMD (m)	-915	915	uniform
turn rate (dps)	-5	5	uniform
advance rate	0	0.8	Gaussian(0.5,0.5)

3.3. Implementation of the Wait Maps

The wait time maps that we produce using the MDP are applied to a discrete event simulator. A baseline DAA algorithm with collision avoidance capability and the DAIDALUS [67] are integrated in the simulator. An unmanned aircraft pilot model [68] is integrated in the simulator to mimic human-pilot response. Reference [68] models the variability of human decision based on three different experimental setups. The model captures pilot response from the beginning of an encounter till safe avoidance. The pilot model uses DAIDALUS to choose avoidance maneuvers. The DAA algorithm onboard the ownship UAS has two primary functions: collision avoidance (CA), and DAA-Pilot mode of operation from the simulator. The combined operation mode allows DAA to override the pilot command in

unusual events. We integrate the allocation agent with the onboard DAA. The allocation agent has the wait map information as resources and utilizes the maps during encounter in the events of communication latency. The agent is activated by default when the operation mode is DAA-Pilot with the provision of manually turning it off. The command blending algorithm in the DAA computer blends the delayed pilot commands with the onboard DAA commands. During the communication latency, the agent matches the current state with a state in the wait map and makes a decision according to (20). The system waits for the optimal wait time extracted from the map until the control is being authorized to the onboard DAA or a delayed pilot command is received. The optimal time is updated when the state is transitioned. The second stage decision making starts when a delayed pilot command is received. The command blending algorithm discussed in Section 2.2 is invoked to determine the maneuver options. We consider two different setup:

- Baseline setup (B): DAA-Pilot mode
- Integrated setup (I): Integrated Agent-DAA-Pilot mode.

The Baseline setup is a standalone DAA setup as presented in Figure 7-a and an integrated setup is the augmented allocation-blend architecture as presented in Figure 7-b. We then design five groups of experiments with different configurations by varying the latency and restricting the use of wait maps within our two setups, as presented in Table 3. The latency is varied according to a Gaussian distribution with a mean around 5 sec and a standard deviation of 3 sec.

Table 3: Experimental Groups.

Setups	Groups	Latency type	Latency (sec)	Wait time (sec)
Baseline	B-1	Constant	4	0
Baseline	B-2	Varying	Gaussian	0
Integrated	IC-1	Constant	5	5
Integrated	ID-1	Constant	4	Map
Integrated	ID-2	Varying	Gaussian	Map

*IC refers to the Integrated setup with a constant wait time and ID refers to the integrated setup with the wait maps.

3.4. Risk Analysis Metric

To evaluate the risk associated with each configuration, we track the number of *LoWC* and *NMAC*. An *NMAC* occurs if

- $R \leq 500$ ft, and

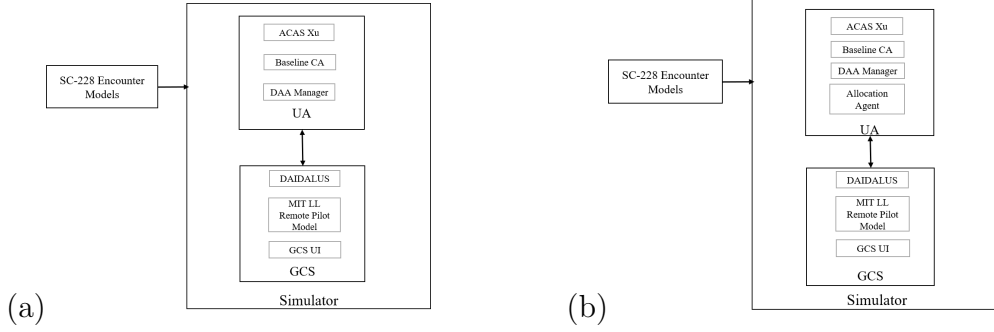


Figure 7: Block diagram of Simulator (a) Baseline Setup and (b) Integrated Setup with Agent

- $H \leq 120$ ft,

where R and H are the horizontal and vertical separation. This pair of separation values is indicated as $NMAC_{threshold}$ later in the paper. We quantify the risk as probabilities of $LoWC$ and probability of NMAC with Monte Carlo approximation. Define $P(LoWC)$ and $P(NMAC)$ as

$$P(LoWC) \approx \frac{1}{K} \sum_{i=1}^K (\{HMD(S(i)), d_h(S(i)), \tau_{mod}(S(i))\} \leq LoWC_{threshold}) \quad (21)$$

and

$$P(NMAC) \approx \frac{1}{K} \sum_{i=1}^K (\{R(S(i)), H(S(i))\} \leq NMAC_{threshold}) \quad (22)$$

where K is the number of sample trajectory points and $S(i)$ is the state vector at the i th time step.

To examine the severity of LoWC, we utilize the metric ‘Penetration Integral’ (PI) [35], which is a measure of penetration into the well clear volume and calculated as

$$PI = \sum_{i=1}^K \min \left(\frac{4000 - HMD(S(i))}{4000}, \frac{450 - VMD(S(i))}{450} \right) \frac{(35 - \tau_{mod}(S(i)))}{35} \Delta T. \quad (23)$$

PI is a scalar measure that quantifies the severity of each LoWC and distinguishes between prolonged severe LoWC and momentary LoWC. A LoWC value less than 2 are considered benign and momentary while a value greater than 10 is considered a significant LoWC [35].

4. Result Analysis

We analyze the results of 10,00 Monte Carlo simulations in this section. Our goal is to efficiently incorporate pilot command without jeopardizing safety. We investigate whether waiting positively improves pilot command incorporation into the system and if the prior

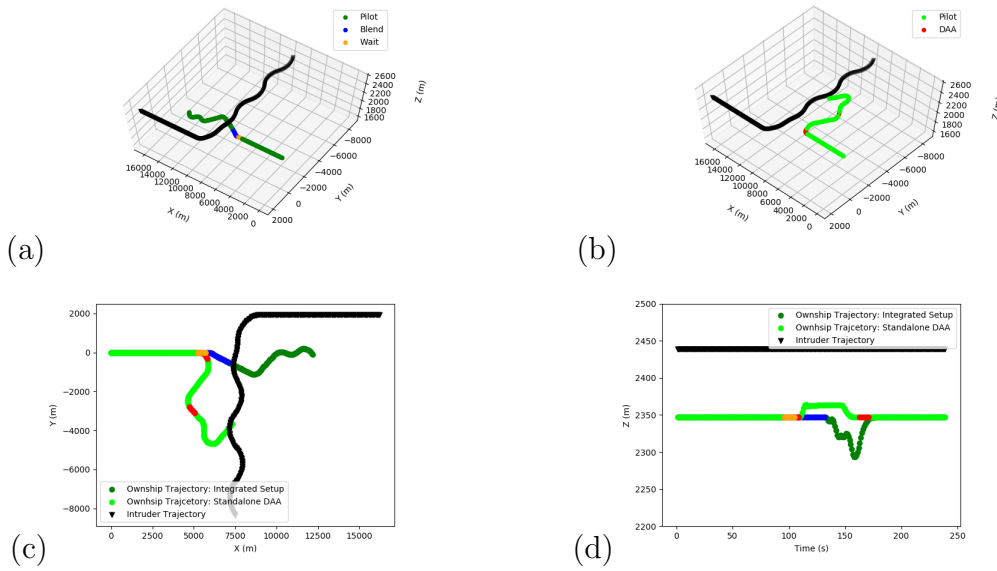


Figure 8: Trajectory analysis with and without the allocation agent in a head-on encounter, the black trajectory represents the intruder. (a) 3-D trajectories with the allocation agent, the orange dots represent the waiting status and the blue dots represent the blended command execution. (b) 3-D trajectories without the allocation agent, the red dots represent the onboard DAA execution. Note that the onboard DAA generates a different maneuver from the pilot’s maneuver shown in (a). (c) The horizontal view illustrates the differences in the trajectories. (d) The vertical view illustrates the vertical differences in the trajectories.

wait maps help allocate the control authority safely. As the UAS waits for pilot commands, it continues to maintain the course, which triggers a question that how safe it is to maintain course in the presence of a dynamic intruder. We analyze the safety from the simulation results in the subsequent sections. We found our augmented allocation-blend architecture improves resolution of diverse encounter scenarios. For example, waiting retain controls for pilot and pilot successfully resolves the encounter. Blending command provides a better avoidance as well as recovery trajectory. Demonstration examples can be found in the supplementary material.

4.1. Pilot Command Incorporation

We inspect command reception and execution in each group and distinguish the changes between the groups. We would like to increase the reception of pilot commands before override taken by the onboard DAA and incorporate the pilot commands to enhance pilot involvement in the resolution process. The waiting action can potentially allow the UAS to receive more pilot commands before a resolution is made. To illustrate how integrating the agent helps pilot and decrease DAA override instances without jeopardizing safety, we provide a representative encounter in Figure 8.

From the Figure 8-c and 8-d, the onboard DAA system without the allocation agent takes over the control and ends up with a trajectory more deviated than the trajectory

produced by the allocation agent. Although the pilot regains control after the DAA takes over, the pilot maneuver changes depending on the situation. With the integrated setup, the UAS waits for the pilot command. When the delayed pilot command is received, the agent invokes the blending algorithm and executes the blended command. As the pilot’s intention is incorporated into the command, upon the pilot’s regaining control, the recovery maneuver is more refined and more on track. With the standalone DAA setup, the DAA takes over the control twice over the encounter. Although in both setups the UAS regains the altitude, the recovery trajectory is not achieved in the DAA setup whereas in the integrated setup the UAS is on track to the original path. The integrated agent improves both the resolution trajectory and the recovery trajectory in this encounter.

The numbers of wait/no wait decisions for each configuration is illustrated in Table 4. The first two groups $B - 1$ and $B - 2$ do not have the allocation agent available in the system. Therefore, during active encounters if a pilot command is unavailable, the system immediately allocates the control to the onboard DAA. With the integrated setup, we have three groups of experiments: the *IC* group refers to the encounters with constant wait time and the *ID* groups refer to the encounters that utilize the wait maps generated from the MDP. The experiment groups in the integrated setups demonstrate how waiting improves the reception of pilot commands and the utility of using a wait map instead of a constant wait time.

On average, the reduction in the DAA allocation between the baseline and the integrated setup is 83.29%. We consider the *ID - 2* group as the comparison standard, as it may represent a more realistic environment, where the system does not have any knowledge of the latency duration. In Figure 9-a, the bar plot illustrates the decrease in the DAA allocation, indicating that the *ID - 2* group has significantly lowered the DAA allocation instances than $B - 2$. This significant decrease in the DAA allocation instances results in an increases in the reception of pilot commands before the resolution is initiated by the onboard DAA.

Table 4: Waiting Status Within Group

Groups	Wait	No Wait (Allocate to DAA)	Percent Reduction	
B-1	0	78842	-	
B-2	0	87153	-	
IC-1	77732	10229	88.26%	*Percent Reduction with
ID-1	59295	21078	75.81%	
ID-2	80650	10278	88.20%	

respect to $B - 2$.

A summary of command generation and reception is presented in Table 5. With the

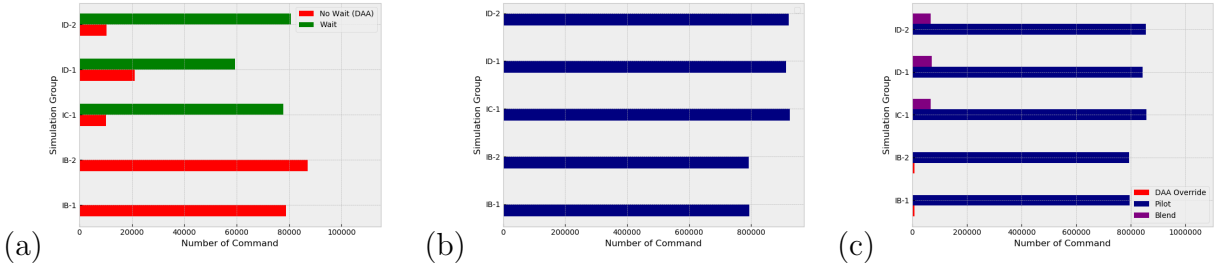


Figure 9: (a) Illustration of wait and no wait (allocate control to DAA) across different groups. The red bar represents onboard DAA commands. Data shows significant reduction in allocation to onboard DAA. (b) Illustration of pilot command reception. (c) Bar graph showing command execution status. Integrated setups have reduced DAA override to zero.

integrated setup, the pilot command reception is increased by 15.81% on average compared to the baseline setup. Comparing the time varying latency groups $B - 2$ and $ID - 2$, we see that the pilot command reception is increased by 16.18%, which includes the commands received before the override resolution.

Table 5: Pilot Command Reception

Groups	Number of Pilot Command Received	Percent Increment
B-1	795163	-
B-2	793529	-
IC-1	924574	16.19%
ID-1	913403	15.10%
ID-2	921993	16.18%

respect to $B - 2$.

*Percent Increment with

The bar graph in Figure 9-b visually illustrates the change in command reception compared to our standard group $ID - 2$. The pilot command reception statistics for the integrated setup in different groups are close. In the group $IC - 1$, the simulator has prior knowledge of the latency that results in a higher number of pilot command reception. Hence, $IC - 1$ has a slightly higher number of reception than our standard $ID - 2$.

The increase in the pilot command reception also results in an increase in pilot involvement in resolution. As the system receives the delayed pilot command, the execution of the command depends on the safety metric that evaluates the feasibility and risk associated with the intended maneuver from the pilot. A positive safety metric indicates a safe maneuver. In the event where the received pilot command is unsafe, the augmented blending algorithm integrates the pilot intended maneuver types to generate DAA maneuvers. Table 6 summarizes the command execution statistics. In the table, a DAA override is an instance where the onboard DAA takes the authority even though a pilot command is available. Figure 9-c visually represents the data in different groups.

Table 6: Command Execution Statistics

Groups	DAA override	Pilot	Blending
B-1	8344	795163	0
B-2	7564	793529	0
IC-1	0	857648	66926
ID-1	0	842914	70489
ID-2	0	853974	68019

The proposed blending algorithm allows the onboard DAA to choose and execute a maneuver that closely matches the pilot preferred maneuver. Executing a maneuver preferred by the pilot is also expected to achieve a better recovery trajectory whenever the pilot regains the full control. We further analyze whether it is possible to find a matched maneuver. As the system waits, the encounter may go in a closer proximity than it would go without waiting. On average, 84% of blended commands were able to find and match the pilot’s exact maneuver type and perform a resolution maneuver in the plane and direction that the pilot had chosen. The remaining 16% of the commands execute maneuvers in the pilot intended plane. In all the scenarios, the pilot preferences in terms of maneuver are augmented into the resolution maneuvers.

4.2. Safety Analysis

The number of LoWC occurrences in each group is illustrated in Figure 10-a. The simulations in group $B - 2$ exhibits the maximum number of LoWC occurrences, where $ID - 2$ has the minimal number of LoWC occurrences. Note that we consider $ID - 2$ as our standard. There are particular scenarios that suffer LoWC in multiple groups. On average, 98% of the encounters that suffer LoWC belong to turning geometry where a high speed intruder converges towards the ownship.

Table 7: Likelihood definition [69]

Frequency	Qualitative	Quantitative P(instance)/flight hour
Frequent, A	Expected to occur routinely	within 1×10^{-3} to 1.00
Probable, B	Expected to occur often	within 1×10^{-3} to 1×10^{-5}
Remote, C	Expected to occur infrequently	within 1×10^{-5} to 1×10^{-7}
Extremely Remote, D	Expected to occur rarely	within 1×10^{-7} to 1×10^{-9}
Extremely Improbable, E	unlikely but it is not impossible	less than 1×10^{-9}

With a total of 666.67 simulation hours (each of the 10,000 encounters lasts $T = 240$ seconds), we calculate the probability of LoWC occurrence per flight hour. The probability of LoWC is calculated using Monte Carlo approximation as

$$P(\text{LoWC}/\text{flight hr}) = \frac{P(\text{LoWC})}{\text{Total flight hours in simulation}}. \quad (24)$$

In Table 7, we recall from the FAA System Safety Handbook [69] how quantitative values of $P(\text{LoWC}/\text{flight hr})$ can be correlated to qualitative measures using FAA safety measure definitions. The qualitative measure is summarized in Table 8 and Figure 10- b visually represents the probability of LoWC calculated from the simulation datasets.

Table 8: Risk Measure per flight hour

Groups	P(LoWC)/flight hr	Qualitative Likelihood
B-1	2.22×10^{-7}	Remote
B-2	2.36×10^{-7}	Remote
IC-1	2.92×10^{-7}	Remote
ID-1	2.77×10^{-7}	Remote
ID-2	2.81×10^{-7}	Remote

The qualitative significance of occurrence according to [69] is that the incidents are expected to occur infrequently and considered remote. With the integrated setup, the system is able to keep the safety margin similar to the DAA only system (without waiting). Although the system results in a slight increase in the probability of the *LoWC* occurrences, the system is able to maintain the safety margin in the same category as the standalone DAA system. This indicates the efficiency of the allocation agent and supports that waiting does not jeopardize safety and degrade risk measure value any more than the baseline system. As all the experiment groups have suffered from LoWC occurrences, we have quantified the severity of each LoWC using the Penetration integral (PI). It measures the severity of LoWC with a positive number. The lower the value, the more instantaneous the LoWC. An illustration of the average PI over each simulation group and the maximum PI value in each simulation is provided in Figure 10-c. The average PI for each simulation group is less than 1 with the maximum value of 3.79 in the *ID-1* group. We further investigate the encounter with the maximum PI and notice that the geometry is very unique, where the intruder has a upside down *V* trajectory as presented in Figure 11. However, this LoWC can also be considered only instantaneous and benign as the value is significantly lower than 10 [35].

We also examine whether the wait actions with the integrated setup induce more trajectory deviation. The mean trajectory deviations in the horizontal and vertical directions are provided in Table 9. The results show that the mean trajectory deviation is almost the same for every setup. In the integrated setup, the UAS waits for the pilot command to arrive, which may induce more aggressive maneuvers, causing the UAS to deviate more from the original trajectory. However, we also observe that some encounters exhibit much higher deviations with the baseline setup.

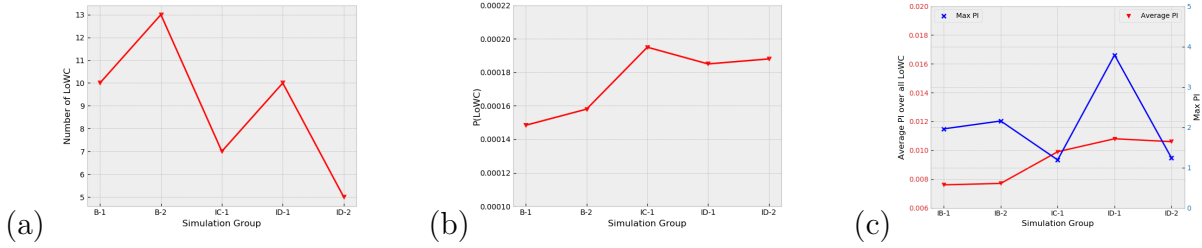


Figure 10: (a) The number of LoWC encounters within 10,000 encounters, $ID - 2$ group has least number of LoWC. (b) Probability of LoWC in sample trajectories in different groups. (c) Average PI in simulation groups and max PI in each group.

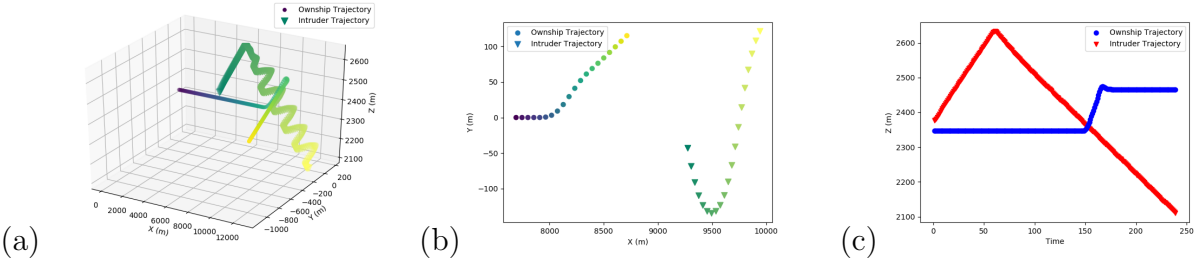


Figure 11: The flight geometry corresponding to the maximum PI. (a) 3-D trajectory: color variation corresponds to time where darker shade indicates starting of the encounter. (b) minimum closure during instantaneous LoWC (horizontal view). (c) Vertical view.

Table 9: Trajectory Deviation

Groups	Horizontal deviation, m	Vertical deviation, m
B-1	1690	184
B-2	1693	183
IC-1	1690	183
ID-1	1693	182
ID-2	1689	182

5. Conclusions

In this paper, we implement an allocation agent in the mixed initiative DAA-pilot platform that dynamically authorizes control between pilot and onboard DAA and blends the received pilot commands in the presence of communication latency. One of the main challenges in the presence of communication latency is the lack of situational awareness and equivalent level of safety without a pilot onboard. The wait map developed from the MDP can potentially allow safe waiting and incorporate more pilot commands in the DAA resolution. To further accommodate pilot commands, a blending algorithm augmenting pilot preference into DAA generated maneuvers is proposed. The integrated system positively improves pilot involvement into the resolutions and decreases override of pilot commands. The results of fast-time Monte Carlo simulations with random latency reflects the effectiveness of

the wait maps and the blending algorithm. The integrated system maintains a similar safe margin as the standalone DAA system used in the simulation.

References

- [1] M. A. Hearst, J. Allen, C. Guinn, E. Horvitz, Mixed-initiative interaction: Trends and controversies, *IEEE Intelligent Systems* 14 (5) (1999) 14–23.
- [2] B. Mok, M. Johns, K. J. Lee, D. Miller, D. Sirkin, P. Ive, W. Ju, Emergency, automation off: Unstructured transition timing for distracted drivers of automated vehicles, in: *2015 IEEE 18th international conference on intelligent transportation systems*, IEEE, 2015, pp. 2458–2464.
- [3] N. Sarter, D. Woods, C. Billings, C. Salvendy, Automation surprises. handbook of human factors and ergonomics, in: *;*, Wiley, 1997.
- [4] M. Li, H. Bai, N. Krishnamurthi, A markov decision process for the interaction between autonomous collision avoidance and delayed pilot commands, *IFAC-PapersOnLine* 51 (34) (2019) 378–383.
- [5] A. Tabassum, H. Bai, C. Kleski, Optimizing unmanned aircraft system decision making for detect-and-avoid with delayed pilot commands, in: *AIAA AVIATION 2020 FORUM*, 2020, p. 2865.
- [6] S. M. Erlien, S. Fujita, J. C. Gerdes, Shared steering control using safe envelopes for obstacle avoidance and vehicle stability, *IEEE Transactions on Intelligent Transportation Systems* 17 (2) (2015) 441–451.
- [7] D. Tran, E. Tadesse, W. Sheng, Y. Sun, M. Liu, S. Zhang, A driver assistance framework based on driver drowsiness detection, in: *2016 IEEE International Conference on Cyber Technology in Automation, Control, and Intelligent Systems (CYBER)*, IEEE, 2016, pp. 173–178.
- [8] M. Walch, T. Sieber, P. Hock, M. Baumann, M. Weber, Towards cooperative driving: Involving the driver in an autonomous vehicle’s decision making, in: *Proceedings of the 8th International Conference on Automotive User Interfaces and Interactive Vehicular Applications*, ACM, 2016, pp. 261–268.
- [9] A. Farjadian, A. Annaswamy, D. Woods, A resilient shared control architecture for flight control, in: *Proceedings of the International Symposium on Sustainable Systems and Technologies*, 2016.

- [10] B. T. Thomsen, A. M. Annaswamy, E. Lavretsky, Shared control between adaptive autopilots and human operators for anomaly mitigation, *IFAC-PapersOnLine* 51 (34) (2019) 353–358.
- [11] R. Chipalkatty, H. Daepf, M. Egerstedt, W. Book, Human-in-the-loop: Mpc for shared control of a quadruped rescue robot, in: *2011 IEEE/RSJ International Conference on Intelligent Robots and Systems*, IEEE, 2011, pp. 4556–4561.
- [12] R. Chipalkatty, G. Droge, M. B. Egerstedt, Less is more: Mixed-initiative model-predictive control with human inputs, *IEEE Transactions on Robotics* 29 (3) (2013) 695–703.
- [13] F. Penizzotto, E. Slawiński, L. R. Salinas, V. A. Mut, Human-centered control scheme for delayed bilateral teleoperation of mobile robots, *Advanced Robotics* 29 (19) (2015) 1253–1268.
- [14] V. A. Shia, Y. Gao, R. Vasudevan, K. D. Campbell, T. Lin, F. Borrelli, R. Bajcsy, Semi-autonomous vehicular control using driver modeling, *IEEE Transactions on Intelligent Transportation Systems* 15 (6) (2014) 2696–2709.
- [15] E. Eraslan, Y. Yildiz, A. M. Annaswamy, Shared control between pilots and autopilots: An illustration of a cyberphysical human system, *IEEE Control Systems Magazine* 40 (6) (2020) 77–97.
- [16] B. Thomsen, A. M. Annaswamy, E. Lavretsky, Shared control between human and adaptive autopilots, in: *2018 AIAA Guidance, Navigation, and Control Conference*, 2018, p. 1574.
- [17] A. Franchi, C. Secchi, M. Ryll, H. H. Bulthoff, P. R. Giordano, Shared control: Balancing autonomy and human assistance with a group of quadrotor uavs, *IEEE Robotics & Automation Magazine* 19 (3) (2012) 57–68.
- [18] S. J. Anderson, S. B. Karumanchi, K. Iagnemma, J. M. Walker, The intelligent copilot: A constraint-based approach to shared-adaptive control of ground vehicles, *IEEE Intelligent Transportation Systems Magazine* 5 (2) (2013) 45–54.
- [19] D. Vanhooydonck, E. Demeester, M. Nuttin, H. Van Brussel, Shared control for intelligent wheelchairs: an implicit estimation of the user intention, in: *Proceedings of the 1st international workshop on advances in service robotics (ASER'03)*, Citeseer, 2003, pp. 176–182.

- [20] J. Philips, J. d. R. Millán, G. Vanacker, E. Lew, F. Galán, P. W. Ferrez, H. Van Brussel, M. Nuttin, Adaptive shared control of a brain-actuated simulated wheelchair, in: 2007 IEEE 10th International Conference on Rehabilitation Robotics, IEEE, 2007, pp. 408–414.
- [21] A. Goil, M. Derry, B. D. Argall, Using machine learning to blend human and robot controls for assisted wheelchair navigation, in: 2013 IEEE 13th International Conference on Rehabilitation Robotics (ICORR), IEEE, 2013, pp. 1–6.
- [22] M. Desai, H. A. Yanco, Blending human and robot inputs for sliding scale autonomy, in: ROMAN 2005. IEEE International Workshop on Robot and Human Interactive Communication, 2005., IEEE, 2005, pp. 537–542.
- [23] J. G. Storms, D. M. Tilbury, Blending of human and obstacle avoidance control for a high speed mobile robot, in: 2014 American Control Conference, IEEE, 2014, pp. 3488–3493.
- [24] T. Inagaki, et al., Adaptive automation: Sharing and trading of control, Handbook of cognitive task design 8 (2003) 147–169.
- [25] R. Takase, J. O. Entzinger, S. Suzuki, Pilot-in-the-loop simulation of simple adaptive fault-tolerant controller, Aerospace Science and Technology 106 (2020) 106125.
- [26] M. Bucolo, A. Buscarino, L. Fortuna, S. Gagliano, Bifurcation scenarios for pilot induced oscillations, Aerospace Science and Technology 106 (2020) 106194.
- [27] C. Kang, C. A. Woolsey, Model-based path prediction for fixed-wing unmanned aircraft using pose estimates, Aerospace Science and Technology 105 (2020) 106030.
- [28] L. Cao, X. Li, Y. Hu, M. Liu, J. Li, Discrete-time incremental backstepping controller for unmanned aircrafts subject to actuator constraints, Aerospace Science and Technology 96 (2020) 105530.
- [29] C. J. Wang, S. K. Tan, K. H. Low, Three-dimensional (3d) monte-carlo modeling for uas collision risk management in restricted airport airspace, Aerospace Science and Technology 105 (2020) 105964.
- [30] N. Zhang, W. Gai, M. Zhong, J. Zhang, A fast finite-time convergent guidance law with nonlinear disturbance observer for unmanned aerial vehicles collision avoidance, Aerospace Science and Technology 86 (2019) 204–214.

- [31] P. Pierpaoli, A. Rahmani, Uav collision avoidance exploitation for noncooperative trajectory modification, *Aerospace Science and Technology* 73 (2018) 173–183.
- [32] R. Radmanesh, M. Kumar, D. French, D. Casbeer, Towards a pde-based large-scale decentralized solution for path planning of uavs in shared airspace, *Aerospace Science and Technology* 105 (2020) 105965.
- [33] Y. Hamada, T. Tsukamoto, S. Ishimoto, Receding horizon guidance of a small unmanned aerial vehicle for planar reference path following, *Aerospace Science and Technology* 77 (2018) 129–137.
- [34] S. Temizer, M. Kochenderfer, L. Kaelbling, T. Lozano-Pérez, J. Kuchar, Collision avoidance for unmanned aircraft using markov decision processes, in: *AIAA guidance, navigation, and control conference*, 2010, p. 8040.
- [35] RTCA Special Committee 228, Minimum operational performance standards (mops) for detect and avoid (daa) systems, 2017 edition (2017).
- [36] A. Tabassum, R. Sabatini, A. Gardi, Probabilistic safety assessment for uas separation assurance and collision avoidance systems, *Aerospace* 6 (2) (2019) 19.
- [37] A. Weinert, S. Campbell, A. Vela, D. Schuldt, J. Kurucar, Well-clear recommendation for small unmanned aircraft systems based on unmitigated collision risk, *Journal of Air Transportation* 26 (3) (2018) 113–122.
- [38] M. G. Wu, S. Lee, C. C. Serres, B. Gill, M. W. Edwards, S. Smearcheck, T. Adami, S. Calhoun, Detect-and-avoid closed-loop evaluation of noncooperative well clear definitions, *Journal of Air Transportation* 28 (4) (2020) 195–206.
- [39] X. Lu, X. Liu, Y. Li, Y. Zhang, H. Zuo, Simulations of airborne collisions between drones and an aircraft windshield, *Aerospace Science and Technology* 98 (2020) 105713.
- [40] Y. Lim, S. Ramasamy, A. Gardi, T. Kistan, R. Sabatini, Cognitive human-machine interfaces and interactions for unmanned aircraft, *Journal of Intelligent & Robotic Systems* 91 (3) (2018) 755–774.
- [41] Y. Lim, T. Samreloy, C. Chantaraviwat, N. Ezer, A. Gardi, R. Sabatini, et al., Cognitive human-machine interfaces and interactions for multi-uav operations, in: *AIAC18: 18th Australian International Aerospace Congress (2019): HUMS-11th Defence Science and Technology (DST) International Conference on Health and Usage Monitoring (HUMS 2019): ISSFD-27th International Symposium on Space Flight Dynamics (ISSFD)*, Engineers Australia, Royal Aeronautical Society., 2019, p. 40.

- [42] J. Y. Chen, E. C. Haas, M. J. Barnes, Human performance issues and user interface design for teleoperated robots, *IEEE Transactions on Systems, Man, and Cybernetics, Part C (Applications and Reviews)* 37 (6) (2007) 1231–1245.
- [43] R. Palacios, J. Hansman, Short-term consequences of radio communications blackout on the us national airspace system, *Aerospace Science and Technology* 29 (1) (2013) 426–433.
- [44] A. Ionita, Input delay investigation in the short period flying qualities criteria, in: *21st Atmospheric Flight Mechanics Conference*, 1996, p. 3424.
- [45] M. Kim, S. Lee, H. Son, Effects of time delay on long range formation control for unmanned aerial vehicles, in: *2016 13th International Conference on Ubiquitous Robots and Ambient Intelligence (URAI)*, IEEE, 2016, pp. 159–162.
- [46] G. Laupré, M. Khaghani, J. Skaloud, Sensitivity to time delays in VDM-based navigation, *Drones* 3 (1) (2019) 11.
- [47] L. R. Salinas, E. Slawiński, V. A. Mut, Complete bilateral teleoperation system for a rotorcraft UAV with time-varying delay, *Mathematical Problems in Engineering* 2015 (2015).
- [48] T. M. Lam, M. Mulder, M. Van Paassen, Collision avoidance in UAV tele-operation with time delay, in: *2007 IEEE International Conference on Systems, Man and Cybernetics*, IEEE, 2007, pp. 997–1002.
- [49] S. K. Armah, S. Yi, Analysis of time delays in quadrotor systems and design of control, in: *Time delay systems*, Springer, 2017, pp. 299–313.
- [50] J. Cox, K. Wong, Predictive feedback augmentation for manual control of an unmanned aerial vehicle with latency, *International Journal of Micro Air Vehicles* 11 (2019) 1756829319869645.
- [51] E. Eraslan, Y. Yildiz, A. M. Annaswamy, Shared control between pilots and autopilots: Illustration of a cyber-physical human system, *arXiv preprint arXiv:1909.07834* (2019).
- [52] A. B. Farjadian, A. M. Annaswamy, D. Woods, Bumpless reengagement using shared control between human pilot and adaptive autopilot, *IFAC-PapersOnLine* 50 (1) (2017) 5343–5348.
- [53] Y. Chen, X.-M. Dong, J.-P. Xue, F.-W. Wang, Robust predictive dynamic control allocation for uncertain actuators, *Control Theory & Applications* 29 (4) (2012) 447–456.

- [54] J. Zhou, M. Canova, A. Serrani, Predictive inverse model allocation for constrained over-actuated linear systems, *Automatica* 67 (2016) 267–276.
- [55] C. Vermillion, J. Sun, K. Butts, Predictive control allocation for a thermal management system based on an inner loop reference model—design, analysis, and experimental results, *IEEE transactions on control systems technology* 19 (4) (2010) 772–781.
- [56] D.-F. Zhang, S.-P. Zhang, Z.-Q. Wang, B.-C. Lu, Dynamic control allocation algorithm for a class of distributed control systems, *International Journal of Control, Automation and Systems* 18 (2) (2020) 259–270.
- [57] Y. Guo, J.-h. Guo, X. Liu, A.-j. Li, C.-q. Wang, Finite-time blended control for air-to-air missile with lateral thrusters and aerodynamic surfaces, *Aerospace Science and Technology* 97 (2020) 105638.
- [58] X. Lang, A. de Ruiter, A control allocation scheme for spacecraft attitude stabilization based on distributed average consensus, *Aerospace Science and Technology* 106 (2020) 106173.
- [59] X. Zhao, Q. Zong, B. Tian, B. Zhang, M. You, Fast task allocation for heterogeneous unmanned aerial vehicles through reinforcement learning, *Aerospace Science and Technology* 92 (2019) 588–594.
- [60] D. Buzorgnia, A. G. Aghdam, A follower-based control allocation in multi-agent networks, in: *2018 Annual American Control Conference (ACC)*, IEEE, 2018, pp. 43–48.
- [61] M. L. Puterman, *Markov Decision Processes.: Discrete Stochastic Dynamic Programming*, John Wiley & Sons, 2014.
- [62] R. W. Beard, T. W. McLain, *Small unmanned aircraft: Theory and practice*, Princeton university press, 2012.
- [63] C. P. Nguyen, A. J. Flueck, Modeling of communication latency in smart grid, in: *2011 IEEE Power and Energy Society General Meeting*, IEEE, 2011, pp. 1–7.
- [64] K. Intharawijitr, K. Iida, H. Koga, Analysis of fog model considering computing and communication latency in 5g cellular networks, in: *2016 IEEE International Conference on Pervasive Computing and Communication Workshops (PerCom Workshops)*, IEEE, 2016, pp. 1–4.

- [65] X. Yang, L. Deng, J. Liu, P. Wei, H. Li, Multi-agent autonomous operations in urban air mobility with communication constraints, in: AIAA Scitech 2020 Forum, 2020, p. 1839.
- [66] S. A. W. Cordwell, Markov decision process (mdp) toolbox for python (2015).
- [67] C. Muñoz, A. Narkawicz, G. Hagen, J. Upchurch, A. Dutle, M. Consiglio, J. Chamberlain, Daidalus: detect and avoid alerting logic for unmanned systems, in: 2015 IEEE/AIAA 34th Digital Avionics Systems Conference (DASC), IEEE, 2015, pp. 5A1–1.
- [68] R. E. Guendel, M. P. Kuffner, D. E. Maki, A model of unmanned aircraft pilot detect and avoid maneuver decisions, Tech. rep., MIT Lincoln Laboratory Lexington United States (2017).
- [69] FAA, FAA System Safety Handbook, Federal Aviation Administration, Washington D.C., 2000.